

## SCATTERING FROM BINARY OPTICS

February 1993

D. W. Ricks  
Naval Air Warfare Center Weapons Division  
China Lake, California, 93555

## ABSTRACT

There are a number of sources of scattering in binary optics: etch depth errors, line edge errors, quantization errors, roughness, and the binary approximation to the ideal surface. These sources of scattering can be systematic (deterministic) or random. In this paper scattering formulas for both systematic and random errors are derived using Fourier optics. These formulas can be used to explain the results of scattering measurements and computer simulations.

## 1.0 INTRODUCTION

For a conventional optical element, such as a mirror, scattering comes from surface roughness or inhomogeneities of surface constants. These surface variations are usually random and are best treated by statistical analysis. In some cases the manufacturing method leads to periodic or quasi-periodic surface features. Single-point diamond turning is an example of a manufacturing process that leaves the surface with accidental periodic surface heights. In these cases the surface bears some resemblance to a diffraction grating and there will be distinct diffraction orders. A randomly rough surface can be regarded as the superposition of an infinite number of diffraction gratings, each with a different grating spacing and hence a different first order diffraction angle. If the *rms* roughness of the surface is much smaller than the wavelength of light, then only the first diffraction order is of any consequence.

In a binary optic the second and higher diffraction orders are important because the depth of the pattern is about one wavelength. In some cases these higher orders of diffraction are desirable, but in many cases anything except the first order can be considered "scattered" light. Scattering from binary optics will also come from the inevitable random surface roughness, just as it does from conventional optics. Binary optics calls for extremely precise positioning and control of etching to insure that each groove is the proper width and depth; errors of fabrication is another source of scattering. Errors of fabrication might be either systematic (deterministic) or random. We shall first consider systematic errors in section 2, and then random errors in section 3.

## 2.0 SYSTEMATIC ERRORS

Systematic errors, or deterministic errors, include: etch depth errors, line edge errors, mask alignment errors, quantization errors, and the shortcomings of an *M*-level binary optic approximation to the ideal continuous phase profile. We shall compare computer simulations to analytical formulas. The computer simulations were performed on a personal computer using the software tool Mathcad 2.5. Where possible these results are compared to the work of others.

## 2.1 GRATINGS

Several types of systematic errors have been investigated in the past in connection with diffraction gratings. When a groove position in the grating varies from the correct position, some energy will be scattered. *Periodic* variations result in the concentration of scattering into spurious diffraction orders called *ghosts*. Ghosts are common in ruled gratings because of periodic errors in turning screws and so forth. An approximate value of the intensity of such ghosts relative to the main diffracted order was given by Rowland in 1893. As presented by Hutley,<sup>1</sup>

$$I_{\text{ghost}}/I(m) = (\pi me/a)^2 \quad (1)$$

where  $m$  is the diffraction order,  $e$  is the maximum departure from the correct position, and  $a$  is the period of the grating. The location of the ghost will depend on the period of the error. As an example, if  $e = 0.1\mu\text{m}$ ,  $a = 1.0\mu\text{m}$ , and  $m = 1$ , then the ghost intensity is approximately ten percent of the main diffraction order. We note in equation (1) that the ghost intensity is proportional to the square of the diffraction order. There should be no ghosts around the zero or central order. Random variations in the position of the grooves cause "grass," a broad spectrum of ghosts of random amplitudes in the plane of the diffraction orders. Scattering from surface roughness, on the other hand, has no preferred orientation and is just as intense out of the plane of incidence as in the plane of incidence.

The diffraction efficiency of a grating is the fraction of the incident energy that is diffracted into a particular order. If only one order is desired, then the diffraction efficiency is a measure of the total unscattered light. We consider a diffraction grating that consists of  $M$  steps per period. All step widths and heights are assumed equal. We use Fourier optics theory and assume that the grating pattern extends to infinity. With these assumptions it can be shown that the relative diffraction efficiency  $\eta(p, M)$  of order  $p$  and with  $M$  levels is

$$\eta(p, M) = \{[\sin(\pi p/M) \sin(\pi p - \phi/2)]/[\pi p \sin(\pi p/M - \phi/2M)]\}^2 \quad (2)$$

where  $\phi/M$  is the change in phase in each step.<sup>2</sup> We note that the highest efficiency for order  $p$  occurs when  $\phi/2 = \pi p$ . Equation (2) is often used for binary optics in general. The assumption is that in a small region of a binary optic the pattern is an approximation to a grating.

## 2.2 ETCH DEPTH ERRORS

The relative loss in diffraction efficiency with etch depth error can be obtained from equation (2). Let  $\eta_{\text{opt}}(p, M)$  be the diffraction efficiency optimized for an order  $p$  and with  $M$  steps. Let  $\epsilon$  be the relative etch depth error, then the phase is given by

$$\phi = 2\pi p(1 + \epsilon).$$

The diffraction efficiency is therefore given by

$$\eta(p, M) = \eta_{\text{opt}}(p, M) \{[\sin(p\epsilon\pi)]/[M \sin(p\epsilon\pi/M)]\}^2. \quad (3)$$

Figure (1) is a plot of the diffraction efficiency for Fresnel zone plate design FZP3A as a function of percent error in etch depth. Table 1 summarizes the design parameters for several Fresnel zone plates. The

TABLE 1. FRESNEL ZONE PLATE DESIGNS

Design	$\lambda(\mu\text{m})$	Levels	$T$	$f(\text{mm})$	$f\#$	$n$	$b(\text{mm})$
FZP1	0.6328	16	316	10	10	1.457	0.35
FZP2A	0.6328	4	79	10	10	1.457	0.35
FZP2B	0.6328	4	2005	254	10	1.457	$\infty$
FZP3A	0.6328	2	40	10	10	1.457	$\infty$
FZP3B	0.6328	2	40	10	10	1.457	0.35
FZP3C	0.6328	2	395	100	10	1.457	3.50
FZP4	10.6	16	19	10	10	4.0	0.35
FZP5	10	16	3360	152.4	3	4.0	$\infty$
FZP6	10	16	300	12.7	1	4.0	$\infty$
FZP7	10	8	1680	152.4	3	4.0	$\infty$
FZP8	10	8	300	12.7	1	4.0	$\infty$

data points were calculated using the approximate Rayleigh-Sommerfeld equation which for a circularly symmetric Fresnel zone plate, on axis, can be written as

$$U(0,0, z) = \sum_j (2\pi z/\lambda i) \phi_j \int_{a_j}^{a_{j+1}} r/(r^2 + z^2) \exp[ik(z^2 + r^2)^{1/2}] dr \quad (4)$$

where,

$$a_j = [2f\lambda/M + (\lambda j/M)^2]^{1/2} \quad (5)$$

$$\phi_j = \exp\{-2\pi i[1 + e]\text{mod}(j, M)/M\} \quad (6)$$

and  $z$  is the distance from zone plate to observation point,  $f$  is the focal length,  $T$  is the maximum number of transition points  $\{a_j\}$ ,  $M$  is the number of levels, and  $e$  is the fractional etch depth error. We define the function  $\text{mod}(j, M)$  as the remainder when  $j$  is divided by  $M$ . For this example the illuminating beam was assumed to be uniform, so the Gaussian beam radius  $b$  (at the  $1/e^2$  points of intensity) is infinite.

For an etch depth error that is uniform across the surface we can use equation (3) for the far-field, paraxial case. In a 2-level Fresnel zone plate an etch depth error of  $e$  will alter the phase over half the surface of the optic (in the grooves only), so we use  $e/2$  for the error term in equation (3). This curve, also shown in figure (1), matches the data very well. Data similar to figure (1) was shown by Cox, et. al.<sup>3</sup>

Uniform etch depth error is one type of systematic error that can occur in a binary optic. The etch depth can also vary across the binary optic; for example each etch depth may be 5 percent deeper than it should be near the center, gradually becoming 5 percent shallower near the edges. This might occur when the narrower grooves near the edges reduce the etching rate. We can model this type of error by writing

$$\phi_j = \exp\{-2\pi i[1 + e(1 - 2a_j/a_T)]\text{mod}(j, M)/M\} \quad (7)$$

for the phase term  $\phi_j$  in equation (4). In computer simulations using the Huygens-Fresnel integral (the approximate Rayleigh-Sommerfeld equation), Goodman and Farn<sup>4</sup> found empirically that the diffraction efficiency of a Fresnel zone plate falls off as the square of the etch error. The effect of etch errors is only a weak function of the number of masks, and it is independent of the f-number and radius. They considered Fresnel zone plates with f-numbers  $f/1$  and  $f/3$  and radii of one and three inches.

Figure (2) shows results identical to Farn and Goodman's data for a 16-level and an 8-level Fresnel zone plate. The relative diffraction efficiency is the peak intensity (equations (4), (5) and (7)) divided by the product of the peak intensity of a perfect lens and the maximum efficiency of an  $M$ -level zone plate (equation (2)). Designs FZP5, FZP6, FZP7, and FZP8 from Table 1 are used in the calculations. The results do not depend on the f-number, and depend only slightly on the number of levels (hence on the number of masks in the fabrication process). Also shown in figure (2) are curves calculated from equation (3), where  $\epsilon = 7/8 e$  for an 8-level zone plate, and  $\epsilon = 15/16 e$  for a 16-level zone plate. The relative etch depth error  $\epsilon$  appears to be the average systematic etch depth error along an axis of the Fresnel zone plate.

A systematic etch depth error decreasing from center to edge should shift the focal position. When the efficiency is calculated at the optimum focal position, then the diffraction efficiency decrease is not nearly as severe as calculated by Farn and Goodman in reference (4). The upper data points in figure (2) shows my calculations for diffraction efficiency at best focus (empirically determined). A good fit to the data is obtained by using equation (3) with  $\epsilon = e/\sqrt{3}$ , which is the rms value of the systematic etch depth error  $e$  along an axis of the Fresnel zone plate. At best focus it is found that the diffraction efficiency is essentially independent of the number of masks, the f-number, and the radius.

### 2.3 LINE EDGE ERRORS

One systematic line edge error would be a linear increase in the position of the transition points. We write the focal length  $f$  from equation (5) in terms of the  $j$ th transition point  $a_j$ , the wavelength  $\lambda$ , and the number of etch levels  $M$ ,

$$f = a_j^2 M/2j\lambda - j\lambda/2M. \quad (8)$$

A uniform expansion of the transition points  $\{a_j\}$  by the factor  $B$  results in a new focal length  $f'$  given by

$$\begin{aligned} f' &= B^2 a_j^2 M / 2j\lambda - j\lambda / 2M \\ &= B^2 f + (B^2 - 1) \lambda j / 2M. \end{aligned} \quad (9)$$

In the paraxial case (i.e., when  $j$  is small) the second term of equation (9) can be ignored and the new focal length is just  $B^2$  times the old focal length. In general the focal length depends on  $j$ , which means there is spherical aberration. The scattering in this case is a spreading of the energy around each diffraction order; and the larger the aperture, the larger the spreading.

Over- or under-exposure of the photoresist during the pattern transfer process can result in systematic line edge errors. Under-exposure results in the grooves being narrower than they should be. Farn and Goodman found that diffraction efficiency (defined as the Strehl ratio) of a Fresnel zone plate falls off linearly with the line edge error, the effect of line edge error is a strong function of the f-number, a weak function of the number of masks and is independent of radius.<sup>4</sup>

Cox et. al. measured the diffraction efficiency of an  $f/10$  Fresnel zone plate in ten "zones" of equal area.<sup>3</sup> The first zone is the central portion of the zone plate, covering ten percent of the entire zone plate. Two zone plates were deliberately under-exposed so that the etched portions were  $1.35 \mu\text{m}$  narrower than they should be. A plot of the measured local diffraction efficiency (fraction of power) is shown in figure (3) for the average of the two zone plates. Also shown is a plot of the calculated local diffraction efficiency in each of the ten "zones" as defined by Cox, et. al.

We expect the diffraction efficiency to decrease with increasing zone number since the error  $e$  becomes relatively more significant as the spacing decreases. In a 2-level zone plate a line edge error represents an area of the zone plate that does not contribute at all to the peak intensity. We therefore subtract the error fraction of a period from the efficiency. In a 2-level zone plate a period is every two transition points. In design FZP3A there are forty transition points, hence four transition points in each of ten "zones" as defined by Cox, et. al. If  $d_i$  is the average period in the  $i$ th "zone", or

$$d_i = (a_{4i+2} - a_{4i} + a_{4i+4} - a_{4i+2}) / 2, \quad (10)$$

then the local diffraction efficiency  $\eta_i$  is approximately given by

$$\eta_i(e) = (1 - e/d_i) [M/\pi \sin(\pi/M)]^2, \quad (11)$$

where  $e$  is the line edge error. When  $e = 0$  equation (11) reduces to the standard formula for diffraction efficiency with no errors (equation (2)). To compare with the Cox data we use the value of  $e = 1.35 \mu\text{m}$  measured by Cox, and we find a good fit using equation (11), as shown in figure (3). The diffraction efficiency is seen in equation (11) to decrease linearly with line edge error and is a strong function of the f-number (the smaller the f-number, the smaller the value of  $d$  in the outer zones) as observed by Farn and Goodman.<sup>4</sup>

#### 2.4 MASK ALIGNMENT ERRORS

The experimental and theoretical work of Cox<sup>3,5</sup> shows that a fixed lateral error, or a mask alignment error, leads to a fall off in diffraction efficiency that is more severe in the outer zones of the zone plate than near the center. In the outer zones a fixed error represents a greater percentage of the pattern and we expect it to cause the greater efficiency decrease. By measuring the local diffraction efficiency of a number of zone plates with design FZP2B, Cox found that the fall off in efficiency is approximately linear from zone to zone. I have plotted in figure (4) the diffraction efficiency in the outer most (i.e. 10th) zone as a function of the mask alignment error. The data points with a small alignment error represent typical fabrication errors, the large alignment error values were intentional. The straight line in figure (4) is given by

$$\eta_{10}(e) = (1 - e/\Delta a_{10,ave}) [M/\pi \sin(\pi/M)]^2 \quad (12)$$

where  $M = 4$  for this 4-level design, and  $\Delta a_{10,ave} = 3.25 \mu\text{m}$  is the mean separation of transition points in the tenth zone. The mean separation is much smaller than the average period used in equation (11). Cox concludes that mask alignment error is more significant than etch depth error or line edge error.

## 2.5 M-LEVEL APPROXIMATION ERRORS

A 100 percent efficient Fresnel zone plate would have a continuously curving profile. Equation (2) indicates that a 16-level binary optic approaches that level of efficiency. How is the energy distributed that is not diffracted into the first order? We know that in the absence of fabrication errors the energy goes into other diffraction orders which will have very low intensity at the first-order focal plane. To calculate the scattering we first reduce the diffraction "ringing," caused by the finite size of the Fresnel zone plate. The amount of energy outside of the central lobe can be minimized by assuming that the Fresnel zone plate is illuminated by a Gaussian beam that has low intensity at the edges of the aperture.

Figure (5) compares the intensity as a function of angle for a cylindrical Fresnel zone plates with 2-, 4-, and 16-levels. We are using designs FZP3B, FZP2A, and FZP1. The intensity is relative to the peak intensity  $I_p$  of a perfect lens with the same f-number. The data has been smoothed by averaging over sixteen successive data points. The first point plotted is the mean of the first sixteen computer generated data points,  $I_1$  to  $I_{16}$ , divided by  $I_p$ . The second point plotted is the mean of  $I_2$  to  $I_{17}$ , divided by  $I_p$ , and so forth. There are 2048 data points for each curve, and the points are spaced at intervals of  $\lambda$ .

We notice in figure (5) that the intensity of the scattered light from the 2-level zone plate seems to drop to the intensity of the 4-level zone plate at about 5.7 degrees. This can be explained as follows. In the 1st-order focal plane the biggest visible difference between the 2-level scattering and the 4-level scattering will be the contribution of the 3rd-order energy. The diffraction efficiency equation (2) indicates that for a 2-level binary optic about 4.5 percent goes into the 3rd-order. The 4-level (and higher) binary optic has no energy in the 3rd-order.

The paraxial focus of the 3rd-order is at  $f/3$ , where  $f$  is the 1st-order focal length. Using geometrical optics the extreme ray from the edge of the zone plate which passes through the 3rd-order focus strikes the 1st-order focal plane at  $x_0'$  given by

$$x_0'/(f - f/3) = (f/2f^{\#})/(f/3) \quad (13)$$

where  $f^{\#}$  is the 1st-order f-number of the zone plate. Hence

$$x_0' = f/f^{\#}. \quad (14)$$

This is the geometric edge of the 3rd-order diffraction in the 1st-order focal plane. As seen from the center of the zone plate this edge makes an angle  $\theta'$ , given by

$$\begin{aligned} \tan\theta' &= x_0'/f \\ &= 1/f^{\#}. \end{aligned} \quad (15)$$

For an  $f/10$  zone plate  $\theta' = 5.7$  degrees, in good agreement with our observation in figure (5).

## 3.0 RANDOM ERRORS

Random errors are processing errors that are statistical in nature. In this section we discuss some random errors that have been noted for gratings. We then derive a formula for random roughness for binary optics. We show that this formula can also be used to calculate the scattering from random etch depth errors and random line edge errors. We compare the formula to computer simulations of random fabrication errors. We use Dammann gratings and Fresnel zone plates as examples.

### 3.1 GRATINGS

From the theory of gratings a random change in form from groove to groove is called "accidental error of amplitude," and is a form of random error independent of grating order.<sup>6</sup> A random error in the position of the groove causes "grass," as mentioned previously. The proportion of the energy scattered into grass is given by<sup>1</sup>

$$I_{\text{grass}}/I(m) = (4\pi m e_{\text{rms}}/a)^2 \quad (16)$$

where  $e_{\text{rms}}$  is the rms error in groove position. According to this formula grass increases as the square of the diffraction order, the same as the intensity for ghosts.

### 3.2 RANDOM ROUGHNESS

We consider now the problem of a binary optic with slightly rough surfaces.<sup>7</sup> We shall consider the binary optic to behave like a grating and use the Fraunhofer diffraction formula. The illumination of the grating will be by a collimated laser beam of wavelength  $\lambda$  and beam radius  $b$ . The beam waist is at the grating. The field at the point  $(x_0, y_0, z)$  is given by (ignoring some unimportant phase terms)

$$U(x_0, y_0, z) = 1/\lambda z \int_{-\infty}^{\infty} \int_{-\infty}^{\infty} \Sigma A_m \exp(2\pi i m x_1/a) \exp[kih(x_1, y_1)(n-1)] \\ \exp[-ik(x_0 x_1 + y_0 y_1)/z] \exp[-(x_1^2 + y_1^2)/b^2] dx_1 dy_1 \quad (17)$$

where  $\Sigma A_m \exp(2\pi i m x_1/a)$  is the Fourier series of the field induced by the binary optic in the  $(x_1, y_1, 0)$  plane,  $a$  is the grating period,  $n$  is the index of refraction of the grating material, and  $h$  is the roughness or surface height variation function. We multiply  $U(x_0, y_0, z)$  by its complex conjugate to obtain the intensity.

We next assume that the distribution of surface heights  $h$  is random with a Gaussian probability; therefore<sup>8</sup>

$$\langle \exp\{ki[h(x_1, y_1) - h(x_2, y_2)](n-1)\} \rangle = \exp\{-[k(n-1)\sigma]^2 [1 - R(x_1 - x_2, y_1 - y_2)]\} \quad (18)$$

where  $\langle \rangle$  denotes the average or expected value,  $\sigma$  is the rms surface roughness and  $R()$  is the autocorrelation function. If we assume that the surface roughness is small,  $k\sigma \ll 1$ , then

$$\exp\{-[k(n-1)\sigma]^2 [1 - R(x_1 - x_2, y_1 - y_2)]\} \approx 1 - [k(n-1)\sigma]^2 [1 - R(x_1 - x_2, y_1 - y_2)]. \quad (19)$$

Next, assume that the autocorrelation function is exponential,

$$R(x_1 - x_2, y_1 - y_2) = \exp\{-[(x_1 - x_2)^2 + (y_1 - y_2)^2]^{1/2}/\tau\} \quad (20)$$

where  $\tau$  is the correlation length. Recognizing that we now have the zero order Hankel Transform of the autocorrelation function we find that

$$\langle I(x_0, y_0, z) \rangle = \langle I_{\text{rough}}(x_0, y_0, z) \rangle + \langle I_{\text{smooth}}(x_0, y_0, z) \rangle \quad (21)$$

where

$$\langle I_{\text{rough}}(x_0, y_0, z) \rangle = [\pi\sigma\tau bk(n-1)/\lambda z]^2 \Sigma |A_m|^2 \{1 + [(2\pi m/a - x_0 k/z)^2 + (y_0 k/z)^2] \tau^2\}^{-3/2}, \quad (22)$$

$$\langle I_{\text{smooth}}(x_0, y_0, z) \rangle = (b^2\pi/\lambda z)^2 \{1 - [k(n-1)\sigma]^2\} \Sigma |A_m|^2 \exp\{-2b^2\pi^2[(x_0/\lambda z - m/a)^2 + (y_0/\lambda z)^2]\}. \quad (23)$$

We can compare these results to the scattering formulas of others by rewriting this expression as the bidirectional transmission distribution function (BTDF). The sine of the specular angle  $\theta_{2,m}$  in the  $m$ th order is given by

$$\sin\theta_{2,m} = \lambda m/a \quad (24)$$

and the sine of the scatter angle is, to the approximations we are using,

$$\sin\theta_s = x_0/z. \quad (25)$$

We define the spatial frequency  $p_m$  by

$$p_m \equiv k(\sin\theta_s - \sin\theta_{2,m}). \quad (26)$$

Along the axis,  $y_0 = 0$ , and we can write the BTDF using equation (22), and equations (24) to (26) by

$$\text{BTDF} = (2k^4/\pi) [\sigma\tau(n-1)/2]^2 \cos\theta_s \Sigma |A_m|^2 / [1 + p_m^2\tau^2]^{3/2}. \quad (27)$$

The typical two-dimensional bidirectional *reflection* distribution function (BRDF) with an exponential autocorrelation function, for normal incidence is given by<sup>9</sup>

$$\text{BRDF} = (2k^4/\pi) (\sigma\tau)^2 \cos\theta_s F(\theta_s) / [1 + p_m^2\tau^2]^{3/2} \quad (28)$$

where  $F(\theta_s)$  is approximately one for small angles, and is exactly one in some theories. Comparing equation (28) with equation (27) we see that one difference is the factor  $[(n-1)/2]^2$ . This difference exists because the phase change on reflection from surface features is proportional to twice the height of the feature, but in transmission the phase change is  $(n-1)$ . The second difference is the term  $\Sigma |A_m|^2$ . Evidently the existence of the grating replicates the scattering pattern around each diffraction order. The amplitude of the scattering is scaled by the amplitude of the diffraction order.

In a similar manner we can derive a formula for one-dimensional random roughness. We shall show that this formula can also predict the scattering from Dammann gratings with random etch depth and random line edge errors. In addition the formula will predict scattering for cylindrical Fresnel zone plates with random etch depth or line edge errors; the results agree well with the average of computer simulations. Equation (22) will predict scattering from circular Fresnel zone plates with random etch depth or line edge errors.

The one-dimensional random roughness formula is derived by assuming that the equations are independent of the  $y_1$ -axis. Instead of a zero order Hankel Transform of the two-dimensional autocorrelation function, we have the Fourier Transform of the one-dimensional autocorrelation function. The end result is

$$\langle I(x_0, y_0, z) \rangle = \langle I_{\text{rough}}(x_0, y_0, z) \rangle + \langle I_{\text{smooth}}(x_0, y_0, z) \rangle \quad (29)$$

where

$$\langle I_{\text{rough}}(x_0, y_0, z) \rangle = [k(n-1)\sigma/\lambda z]^2 b\tau \sqrt{(2\pi)\Sigma |A_m|^2} [1 + \tau^2(kx_0/z - 2\pi m/a)^2]^{-1} \quad (30)$$

$$\langle I_{\text{smooth}}(x_0, y_0, z) \rangle = (b/\lambda z)^2 \pi \{1 - [k(n-1)\sigma]^2\} \Sigma |A_m|^2 \exp\{-2b^2\pi^2[x_0/\lambda z - m/a]^2\}. \quad (31)$$

We recall that  $\sigma$  is the rms roughness,  $\tau$  is the correlation length,  $k = 2\pi/\lambda$ ,  $b$  is the radius of the Gaussian beam,  $n$  is the refractive index of the substrate,  $a$  is the period of the grating, and  $|A_m|^2$  (as it turns out) is the diffraction efficiency of the  $m$ th order.

### 3.3 ETCH DEPTH ERRORS

We now consider etch depth errors where the etch depth varies randomly from groove to groove. We can consider Dammann gratings and cylindrical Fresnel zone plates as one-dimensional rough surfaces. Circular Fresnel zone plates are two-dimensional.

### 3.3.1 DAMMANN GRATING

Dammann gratings are convenient to consider because they are simple two-level binary optics where the diffraction orders are spatially separated. We consider a number of designs, as shown in Table 2.

TABLE 2. DAMMANN GRATING DESIGNS

Design	Transition points		depth $h(\mu\text{m})$	period $a(\mu\text{m})$	$\lambda$ $(\mu\text{m})$	Equal intensity (orders)
	$a_1(\mu\text{m})$	$a_2(\mu\text{m})$				
DG1	43.02	86.96	0.545	200	0.633	0, $\pm 1$ , $\pm 2$ , $\pm 3$
DG2	43.02	86.96	9.129	200	10.6	0, $\pm 1$ , $\pm 2$ , $\pm 3$
DG3	10.75	21.74	0.545	50	0.633	0, $\pm 1$ , $\pm 2$ , $\pm 3$
DG4	13.74	30.06	1.23	60.12	10.6	

Figure (6) shows the relative intensity of Dammann grating design DG1 with a random etch depth error. In addition to the values in Table 2,  $b = 4.5$  mm,  $f = 1.82$  m, and  $n = 1.45702$ , except for DG4 where  $b = 2.5$  mm and  $n = 3.4178$ . The standard deviation of the error is  $\delta = 0.01 \mu\text{m}$ . The intensity profile was calculated with four sets of random numbers and the results were averaged together. The results were also smoothed by averaging over sixteen data points, and normalized by dividing by the peak intensity in the error-free case. In figure (6) the zero diffraction order is at zero degrees, and the next four positive diffraction orders are also shown. The negative diffraction orders would be similar and are not plotted.

Also shown in figure (6) is a plot of equation (29). The correlation length  $\tau$  we estimate to be approximately equal to the width of the etched portion of the Dammann grating. In this portion the correlation is unity, falling off to zero outside of the etched area. For design DG1 there are two etched portions per period; the width of each is  $86.96 - 43.02 = 43.94$ , so we set  $\tau = 44$ . The rms roughness  $\sigma$  is

$$\begin{aligned}\sigma &= (\delta^2\tau/a + 0 + \delta^2\tau/a + 0)^{1/2} \\ &= \delta (2\tau/a)^{1/2}.\end{aligned}\quad (32)$$

In figure (7) the standard deviation of the etch error has been increased to  $\delta = 0.1 \mu\text{m}$ . The average of four computer simulations using the Fresnel diffraction formula is shown together with the 1-D roughness equation (29). The value of  $\tau$  is again  $44 \mu\text{m}$ , and we use equation (31) to calculate the rms roughness. It appears to be a good fit. We see from equation (29), and it is confirmed in the computer simulations illustrated in figures (6) and (7), that the scattering is proportional to  $\delta^2$ , since  $\delta$  and  $\sigma$  are linearly related through equation (31). The diffraction efficiency can be given by equation (31), which indicates that for random etch depth errors with two etched surfaces per period, the diffraction efficiency decreases by

$$\begin{aligned}\eta &= \eta_0 \{1 - [k(n-1)\sigma]^2\} \\ &= \eta_0 \{1 - (2\tau/a)[k(n-1)\delta]^2\}\end{aligned}\quad (33)$$

using equation (32). The efficiency with no errors is  $\eta_0$ , and is given by equation (2).

What effect does wavelength have on the scattering? Consider design DG2, which has the same transition points (hence the same pattern), but differs in the design wavelength and etch depth. The relative intensity profile is shown in figure (8), along with a plot of the one-dimensional scattering formula (29). Formula (29) agrees as well with computer simulations for the  $10.6 \mu\text{m}$  wavelength as for the  $0.6328 \mu\text{m}$  wavelength. The etch depth error has a standard deviation of  $0.1 \mu\text{m}$ , the same as the error illustrated in figure (7), but the relative scattering is much less. This is in keeping with the prediction of equations (30) and (31) that the relative scattering is

$$\langle I_{\text{rough}}(x_0, y_0, z) \rangle / I_{\text{peak}} = [k(n-1)\sigma/\lambda z]^2 b \tau \sqrt{(2\pi) \sum |A_m|^2 [1 + \tau^2(kx_0/z - 2\pi m/a)^2]^{-1} / (b/\lambda z)^2 \pi |A_{\text{peak}}|^2}$$

$$= [k(n-1)\sigma]^2 \tau \sqrt{2} \sum |A_m/A_{\text{peak}}|^2 [b/\pi + b/\pi \tau^2 (kx_0/z - 2\pi m/a)^2]^{-1} \quad (34)$$

assuming there is not much overlap of energy between diffraction orders. We see from equation (34) that the relative scattering is proportional to  $(k\sigma)^2$  and therefore proportional to  $(\delta/\lambda)^2$ , as we can also see by comparing figures (8) and (7).

### 3.3.2 CYLINDRICAL FRESNEL ZONE PLATES

Continuing with our examination of random etch depth errors, we now look at cylindrical Fresnel zone plates. This type of zone plate will show one-dimensional scattering characteristics. The cylindrical Fresnel zone plate creates a line focus (at  $x_0 = 0$ ) for each diffraction order at a distance from the zone plate that depends on the diffraction order. We shall concern ourselves only with the scattering from roughness in the first diffraction order; in the 1st-order focal plane scattering from other diffraction orders is insignificant. The relative scatter intensity from roughness is therefore (using equation (34)),

$$\langle I_{\text{rough}}(x_0, y_0, z) \rangle / I_{\text{peak}} = [k(n-1)\sigma]^2 \tau \sqrt{2} [b/\pi + b/\pi (\tau kx_0/z)^2]^{-1} \quad (35)$$

for the cylindrical Fresnel zone plate.

As before, the correlation length  $\tau$  is the mean width of the etched portions;

$$\tau = \text{mean}\{a_{j+1} - a_j\} \quad (36)$$

which for design FZP1 gives  $\tau = 1.58 \mu\text{m}$ . For the Fresnel zone plates all levels were assumed to have some etch depth error, so the mean is taken over all intervals. This also implies that  $\sigma = \delta$ . Figure (9) should be compared to figure (10) where the standard deviation of the etch depth error is  $\delta = 0.1 \mu\text{m}$  and  $\delta = 0.01 \mu\text{m}$ , respectively. The scattering drops two orders of magnitude with one order of magnitude decrease in the error. Again equation (35) provides a good prediction of the average value of the scattering at a particular angle. Equation (35) predicts that the scattering is proportional to  $\sigma^2$ , and  $\sigma^2 = \delta^2$  in this case.

A 4-level Fresnel zone plate (FZP2A) shows behavior similar to the 16-level zone plates just considered. Figure (11) illustrates this case when the standard deviation of the etch depth error is  $\delta = 0.1 \mu\text{m}$ . A plot of equation (35) is shown for comparison. Equation (36) gives  $\tau = 6.33 \mu\text{m}$ ; and  $\sigma = \delta$ . The random scattering in this case is less than the systematic error for angles greater than about three degrees; averaging is necessary to reveal the scattering. The gaps in the curve indicate where the average intensity with etch depth errors is less than the intensity without etch depth errors. Further averaging should make the relative scatter intensity converge to the plot of equation (35).

### 3.3.3 CIRCULAR FRESNEL ZONE PLATES

We now consider random etch depth errors in circular Fresnel zone plates. In this case we must use the two-dimensional roughness scattering formula, equation (21). For our purposes here we want the scatter intensity from the "rough" part divided by the peak intensity of the smooth part in the absence of roughness. Using equations (22) and (23) we find

$$\langle I_{\text{rough}}(x_0, y_0, z) \rangle / I_{\text{peak}} = [k(n-1)\sigma\tau/b]^2 [1 + (\tau kx_0/z)^2 + (\tau ky_0/z)^2]^{-3/2} \quad (37)$$

for the two-dimensional or circular Fresnel zone plate. The rms roughness  $\sigma$  will be, as before, equal to the standard deviation of the etch depth error,  $\delta$ . The correlation length will again be given by equation (36).

The relative scattering for the circular Fresnel zone plate with design FZP1 is shown in figure (12). The relative scattering in the two-dimensional case is much less than the relative scattering in the one-dimensional case (figure (9)) for the same average etch depth error.

Design FZP1 also has much less relative scattering than design FZP4, shown in figure (13). What is the

reason for this? There are three terms in equation (37) which change from design FZP1 to FZP4;  $\tau$ ,  $\lambda$ , and  $n$ . The correlation length  $\tau$  in turn is a function of the wavelength  $\lambda$ , the number of levels  $M$ , and the f-number  $f^\#$ . We now derive an approximate value for  $\tau$ . If the f-number is not too small we can approximate the transition point  $a_j$  from equation (5) by using the paraxial approximation,

$$a_j^2 \approx 2\lambda f_j / M.$$

Hence,

$$a_{j+1}^2 - a_j^2 \approx 2\lambda f / M$$

and therefore

$$a_{j+1} - a_j \approx 2\lambda f / (Ma_{j+1} + Ma_j).$$

We have then that

$$\begin{aligned} \tau = \text{mean}(a_{j+1} - a_j) &\approx [2\lambda f / M] \text{mean}(1/[a_{j+1} + a_j]) = 2\lambda f / Ma_\tau \\ \tau &\approx 4\lambda f^\# / M. \end{aligned} \quad (38)$$

We see that the term  $k\tau$  in equation (37) is approximately the same in both design FZP1 and FZP4, hence the difference in relative scattering levels is due solely to the difference in refractive index  $n$  of the two designs.

### 3.4 LINE EDGE ERRORS

We now examine the effects of random line edge error in Dammann gratings and Fresnel zone plates. The location of the line edge is made random by adding  $e_j$  to the transition point  $a_j$ , where  $e_j$  is a random number with mean of zero and standard deviation  $\delta$ . Our random roughness formulas were derived under the assumption of a small random phase shift to the surface, but we will attempt to use these formulas for the random line edge errors.

A random line edge error could be regarded as a perturbation from the ideal pattern. The height of the perturbation is the step height,  $h$ . The rms roughness  $\sigma$  is then the square root of the average amount of height perturbation, or

$$\sigma = [m \langle w \rangle h^2 / a]^2 \quad (39)$$

where  $m$  is the number of edges which vary from their proper positions in a period  $a$ , and  $\langle w \rangle$  is the mean width of the perturbations. For a uniform probability over either the interval  $[0, \delta/\sqrt{3}]$  or  $[-\delta/\sqrt{3}, 0]$ ,

$$\langle w \rangle = \delta(\sqrt{3})/2 \quad (40)$$

and  $\delta$  is the standard deviation of the error over that interval.

In the derivation of the rms roughness formula we assumed a two-sided exponential probability density function,  $(1/2\tau) \exp(-|x|/\tau)$ . Hence the standard deviation  $\delta$  is related to the correlation length  $\tau$  by

$$\begin{aligned} \delta &= [(1/2\tau) \int_{-\infty}^{\infty} x^2 \exp(-|x|/\tau) dx]^{1/2} \\ &= \tau\sqrt{2}. \end{aligned} \quad (41)$$

With  $\sigma$  and  $\tau$  now given by equations (39), and (41), we can compare the computer simulations of random line edge error to plots using the roughness formulas.

### 3.4.1 DAMMANN GRATINGS

We begin our examples of random line edge errors with the Dammann gratings. Figure (14) shows the relative intensity versus angle for Dammann grating DG1 with line edge error  $\delta = 1 \mu\text{m}$ . A plot of the roughness formula (29) is also shown (it is almost constant at  $10^{-4}$ ). There are four edges per period in design DG1, so  $m = 4$  in equation (39). The step height  $h$  is given in Table 2. The scattering predicted by equation (29) appears to be a little high compared to the computer simulation, possibly because the assumption made in the derivation that  $h$  is small compared to  $\lambda$  is not very good. Figure (15) shows the case for  $\delta = 0.1 \mu\text{m}$ . Equation (30) correctly predicts an increase in scattering of magnitude 100 when  $\delta$  is increased by a factor of 10. To see this in equation (30) we note that

$$\begin{aligned} \langle I_{\text{rough}}(x_0, y_0, z) \rangle &\propto \sigma^2 \tau \\ &\propto \langle w \rangle \tau \\ &\propto \delta^2 \end{aligned} \quad (42)$$

using equations (39), (40), and (41). When the period is decreased by a factor of four (design DG3), the scattering increases by a factor of four (not shown here). The scattering is proportional to  $\sigma^2$  in equation (30), and therefore proportional to  $1/a$ , according to equation (39).

When the wavelength is increased, and the step height is increased proportionally (design DG2), the relative scattering intensity remains the same for random line edge errors. The roughness formula (34) predicts this since the relative scattering is proportional to  $(\sigma k)^2$ , which is proportional to  $(h/\lambda)^2$  by equation (39).

Figure 16 is a comparison of the roughness formula with measured data. The design is the same as DG1 except the etch depth was (accidentally)  $0.662 \mu\text{m}$  instead of  $0.545 \mu\text{m}$ . This results in a reduction of the zero order about a factor of ten from the design value. Measurements using a WYKO profilometer indicate a *rms* roughness of about  $0.43 \text{ nm}$ , too little to explain the measured scattering. The random etch depth error was measured to be about  $1.0 \text{ nm}$ , which could account for some of the scattering. A random line edge error with standard deviation of  $0.025 \mu\text{m}$ , when added to the etch depth error, gives a good approximation to the measured scattering. This level of random line edge error was too small to be measured with the WYKO, and is less than a typical manufacturing error.

Another comparison of measured data and the roughness formula is shown in figure (17) for design DG4. The *rms* roughness of the lands was about  $1.0 \text{ nm}$ , but the grooves had a slope giving an effective roughness of  $27.6 \text{ nm}$ . Since this slope was periodic we would expect a systematic error, rather than a random error. Plotting these values of etch depth roughness shows  $1.0 \text{ nm}$  accounts for only a small part of the measured scattering, and  $27.6 \text{ nm}$  predicts orders of magnitude more scattering than was measured. A line edge error with standard deviation of  $0.03 \mu\text{m}$  agrees reasonably well with the scattering measurement.

### 3.4.2 CYLINDRICAL FRESNEL ZONE PLATES

We now consider random line edge errors in Fresnel zone plates. Figure (18) is a plot of the relative scatter intensity of a cylindrical zone plate, design FZP1. The systematic error part of a 16-level zone plate has been subtracted out. We add a random number  $e_i$  to each transition point  $a_i$ . To plot the roughness equation we use the same formulas for  $\tau$  and  $\sigma$  as we did for Dammann gratings. We interpret equation (39) using  $m = T$  for the number of transition points or edges in the half-width or radius  $a$  of the design. We could write

$$\sigma = h[\delta(\sqrt{3})T\Gamma^\#/\lambda]^{1/2} \quad (43)$$

using equations (39) and (40). The relative scattering increases by a factor of 100 when the line edge errors increase by a factor of 10, as it does for Dammann gratings.

Design FZP2 has one fourth the transition points of design FZP1, but the step heights are four times

as high, since

$$h = \lambda / [(n - 1)M]. \quad (44)$$

Roughness is proportional to  $h/T$ , as we see from equation (43), so design FZP2 has twice the roughness of design FZP1, and therefore four times the scattering for the same random line edge error. Computer simulations confirm this prediction of the roughness formula.

There is less scattering from design FZP4 than design FZP1. It appears to be a result of differences in the factors  $\lambda$ ,  $T$ , and  $n$ . The number of transition points  $T$  is reduced approximately in proportion to  $\lambda$ . The step height is increased in proportion to  $\lambda$ , but decreased in proportion to  $(n - 1)$ . We have from equations (30), (43), and (44)

$$\begin{aligned} I_{\text{rough}} &\propto [(n - 1)\sigma/\lambda]^2 \\ &\propto (n - 1)^2 h^2 T/\lambda^2 \\ &\propto (n - 1)^2 [\lambda/(n - 1)]^2 1/\lambda^3 \\ &\propto 1/\lambda. \end{aligned} \quad (45)$$

We see that the refractive index  $n$  doesn't really affect the scattering intensity for line edge errors, and the net result is that the scattering is inversely proportional to the wavelength. However, if one particular design were used at two wavelengths, then  $T$  and  $\sigma$  would be constant, and the scattering would be proportional to  $1/\lambda^2$ .

### 3.4.3 CIRCULAR FRESNEL ZONE PLATES

Lastly we consider designs FZP1 and FZP4 for random line edge errors in circular Fresnel zone plates. The intensity is found using random numbers  $e_j$  added to the transition points  $a_j$ . These results are compared to the roughness formula (37). As before, the correlation length is  $\delta/\sqrt{2}$ , and the *rms* roughness  $\sigma$  is the *rms* surface height with respect to the design step height. For a circular Fresnel zone plate

$$\begin{aligned} \sigma &= \{\Sigma_j [(a_j + \langle w \rangle)^2 - a_j^2] (h/a_T)^2\}^{1/2} \\ &= (h/a_T) [T \langle w \rangle^2 + 2 \langle w \rangle \Sigma_j a_j]^{1/2} \\ &= (h/a_T) [T \delta^2 3/4 + \delta \sqrt{3} \Sigma_j a_j]^{1/2}. \end{aligned} \quad (46)$$

Figure (19) shows that the relative intensity of the scatter is down six or seven orders of magnitude from the peak intensity, even for a fairly large line edge error of  $1 \mu\text{m}$  standard deviation. As in the one-dimensional case, the roughness formula predicts a decrease in relative scattering proportional to  $1/\lambda$  for optimized designs.

## 4.0 CONCLUSIONS

Using Fourier optics methods some formulas for scattering from binary optics have been developed. These formulas are similar to standard random roughness formulas used to predict scattering from smooth surfaces. The formulas are shown to agree reasonably well with computer simulations and actual measurements.

## 5.0 REFERENCES

1. M.C. Hutley, *Diffraction Gratings*, Academic Press, 1982.
2. G.J. Swanson, "Binary Optics Technology: Theoretical Limits on the Diffraction Efficiency of Multilevel Diffractive Optical Elements," Massachusetts Institute of Technology Lincoln Laboratory, Technical Report 914, 1 March 1991.

3. J.A. Cox, T. Werner, J. Lee, S. Nelson, B. Fritz, and J. Bergstrom, "Diffraction efficiency of binary optical elements," *Computer and Optically Formed Holographic Optics*, SPIE Proceedings Vol. 1211, pp. 116-124 (1990).
4. M.W. Farn, J.W. Goodman, "Effect of vlsi fabrication errors on kinoform efficiency," *Computer and Optically Formed Holographic Optics*, SPIE Proceedings Vol. 1211, pp. 125-136 (1990).
5. J.A. Cox, B. Fritz, and T. Werner, "Process error limitations on binary optics performance," *Computer and Optically Generated Holographic Optics (Fourth in a Series)*, SPIE Proceedings Vol. 1555, pp. 80-88 (1991).
6. C.M. Sparrow, "Theory of Imperfect Gratings," *Astrophysical Journal*, Vol. XLIX No. 2, March 1919.
7. This derivation was worked out with the help of Dr. Merle Elson and Larry Chizek. It was published in Larry's thesis "Near-Angle Scattering and Binary Optics," Naval Postgraduate School, December 1989. The results were given in D.W. Ricks and L.V. Chizek, "Light scattering from binary optics," *Computer and Optically Formed Holographic Optics*, Ivan Cindrich and Sing H. Lee, Editors, Proc. SPIE 1211, 24-37 (1990).
8. C.C. Sung and J.A. Holzer, "Scattering of Electromagnetic Waves from a Rough Surface," *Applied Physics Letters*, Vol. 28, No. 8, pp. 429-431, 1976.
9. E.L. Church, H.A. Jenkinson, and J.M. Zavada, "Measurement of the finish of diamond-turned metal surfaces by differential light scattering," *Optical Engineering*, Vol. 16 No. 4, July-August 1977.

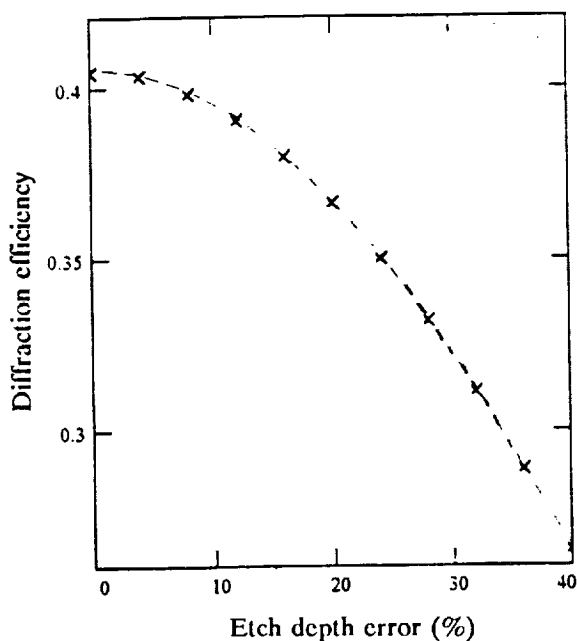


FIGURE 1. Diffraction efficiency versus uniform etch depth error (%), Fresnel zone plate (FZP3A). Computer simulation (X) compared to equation (3).

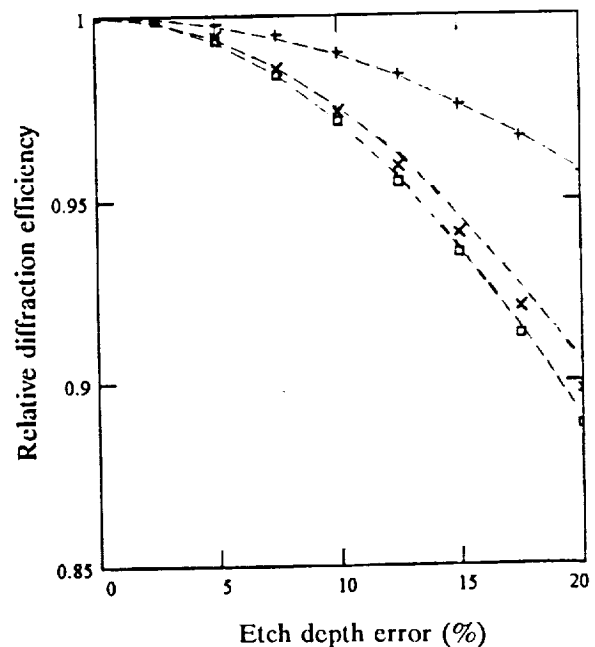


FIGURE 2. Relative diffraction efficiency versus systematic error (%). 16-level (0), 8-level (X), and best focus (+); compared to equation (3).

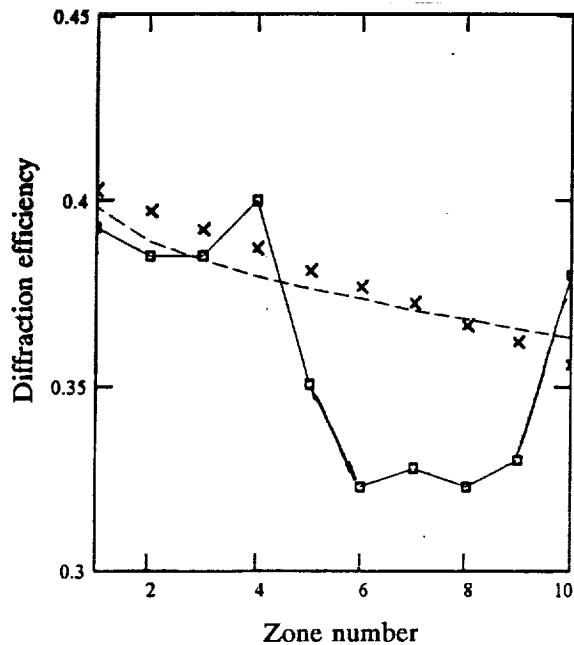


FIGURE 3. Diffraction efficiency versus zone number. Comparing Rayleigh-Sommerfeld (X), equation (11), and data (-0-0-) from ref. (3).

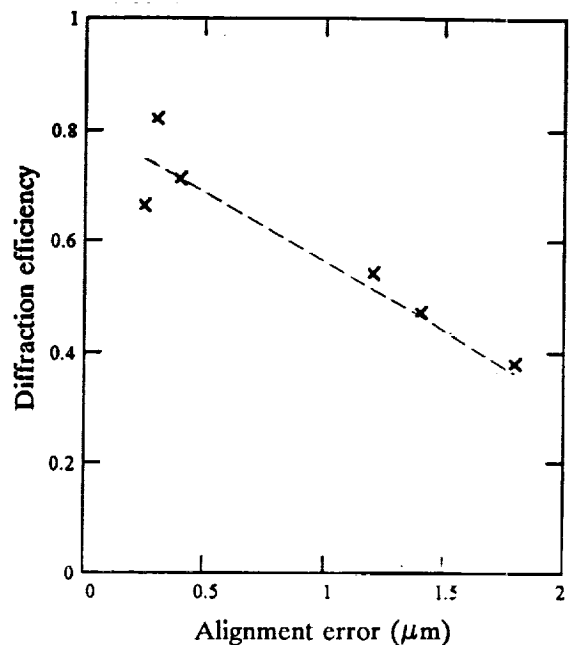


FIGURE 4. Diffraction efficiency in the outer zone versus mask alignment error ( $\mu\text{m}$ ). Equation (12) compared to measured data (X) from ref. (5).

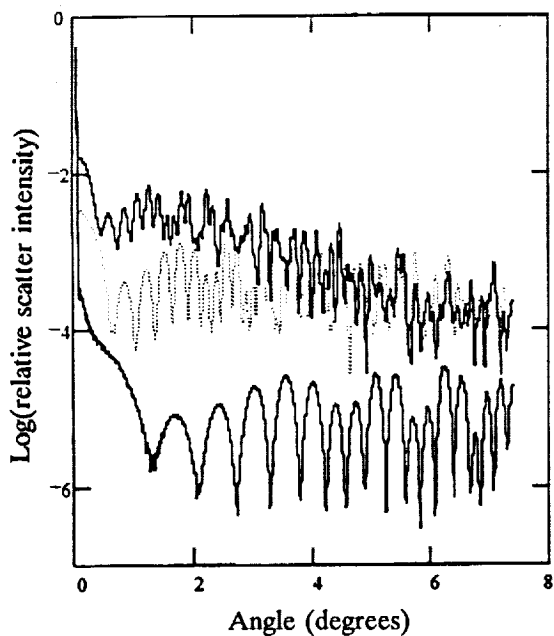


FIGURE 5. Relative scatter intensity versus scattering angle. Cylindrical Fresnel zone plate; 16-level (bottom), 4-level, and 2-level (top).

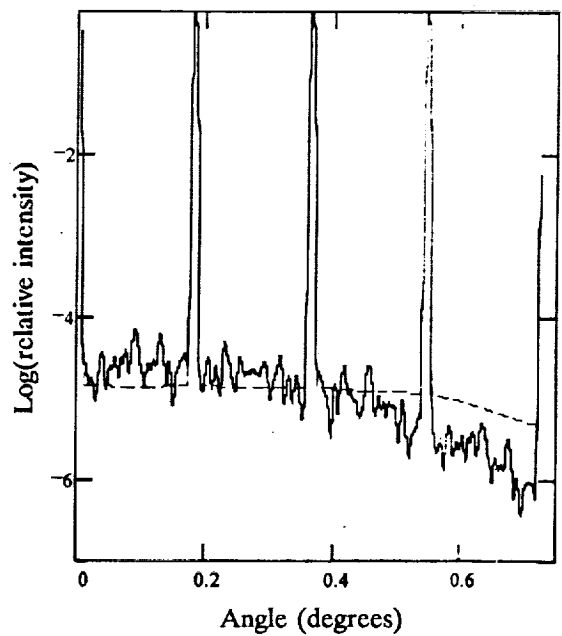


FIGURE 6. Relative intensity, Dammmann grating (DG1). Etch depth error  $\delta = 0.01 \mu\text{m}$ . Compared to 1-D roughness scattering formula.

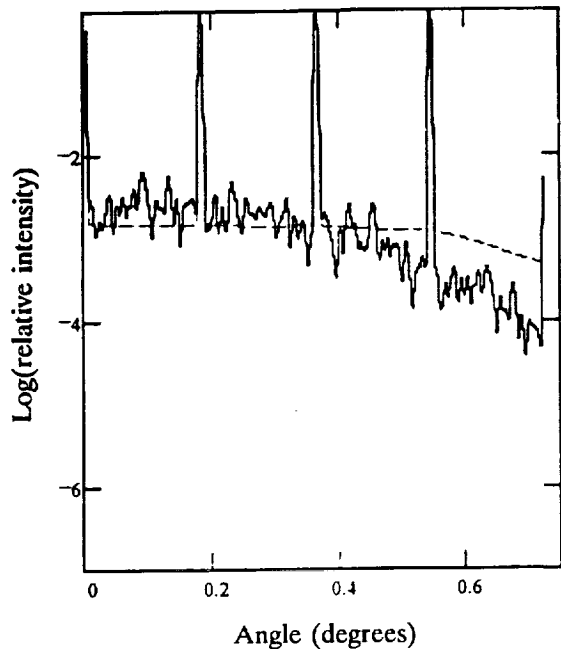


FIGURE 7. Relative intensity, Dammann grating (DG1). Etch depth error  $\delta = 0.1 \mu\text{m}$ . Compared to 1-D roughness scattering formula.

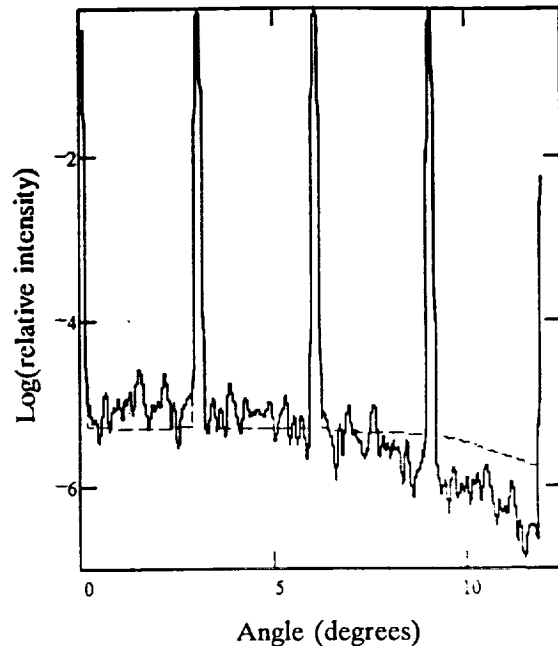


FIGURE 8. Relative intensity, Dammann grating (DG2). Etch depth error  $\delta = 0.1 \mu\text{m}$ . Compared to 1-D roughness scattering formula.

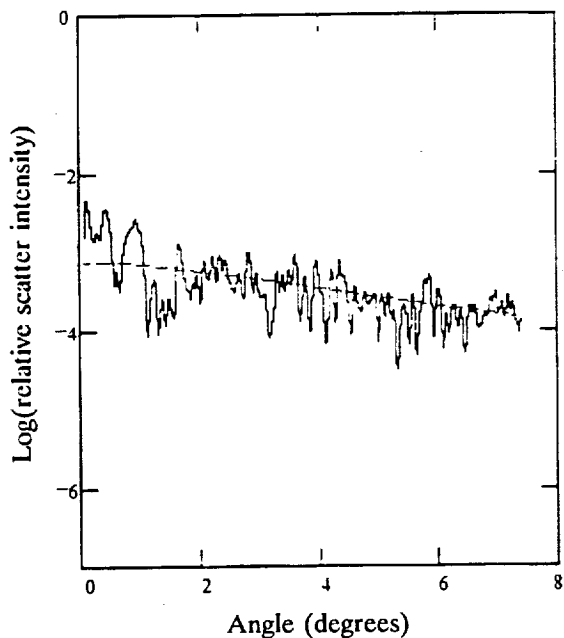


FIGURE 9. Relative scatter intensity, cylindrical Fresnel zone plate (FZP1). Etch depth error  $\delta = 0.1 \mu\text{m}$ . Compared to 1-D scattering formula.

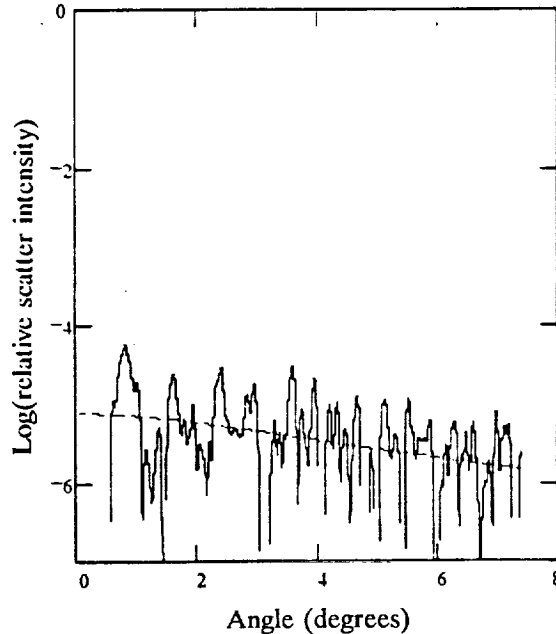


FIGURE 10. Relative scatter intensity, cylindrical Fresnel zone plate (FZP1). Etch depth error  $\delta = 0.01 \mu\text{m}$ . Compared to 1-D scattering formula.

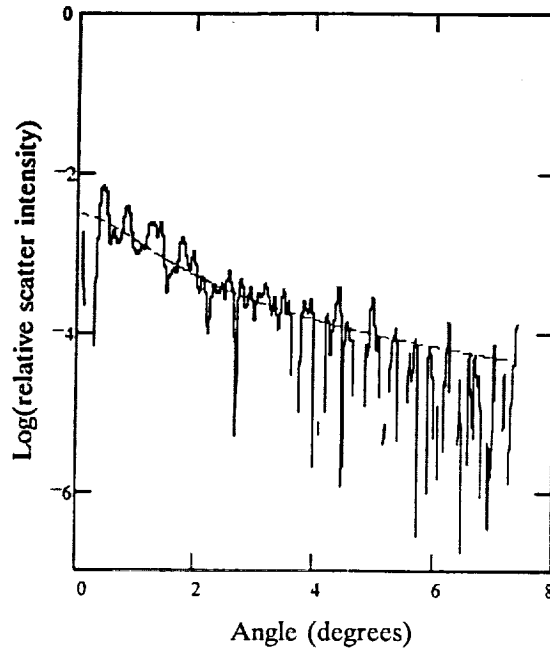


FIGURE 11. Relative scatter intensity, cylindrical Fresnel zone plate (FZP2A). Etch depth error  $\delta = 0.1 \mu\text{m}$ . Compared to 1-D roughness scattering formula.

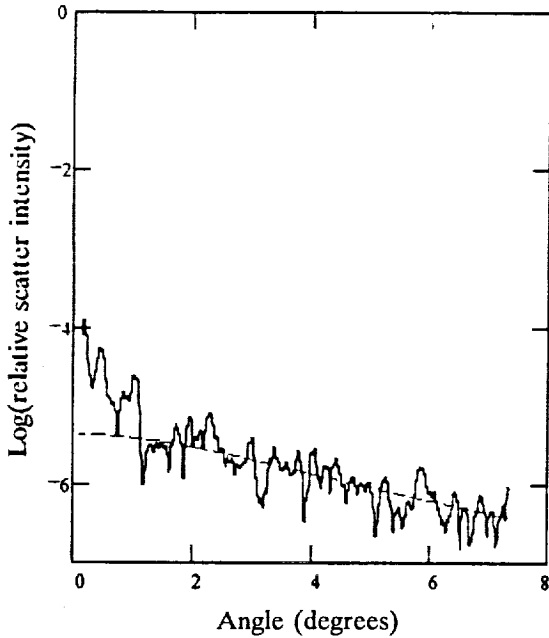


FIGURE 12. Relative scatter intensity, circular Fresnel zone plate (FZP1). Etch depth error  $\delta = 0.1 \mu\text{m}$ . Compared to 2-D scattering formula.

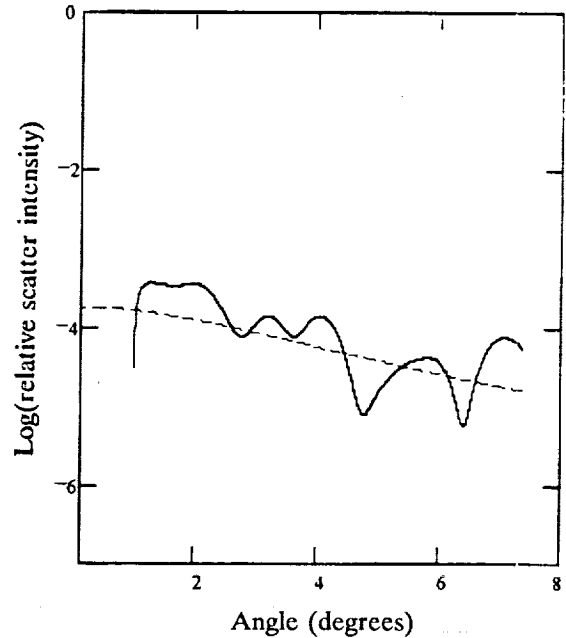


FIGURE 13. Relative scatter intensity, circular Fresnel zone plate (FZP4). Etch depth error  $\delta = 0.1 \mu\text{m}$ . Compared to 2-D scattering formula.

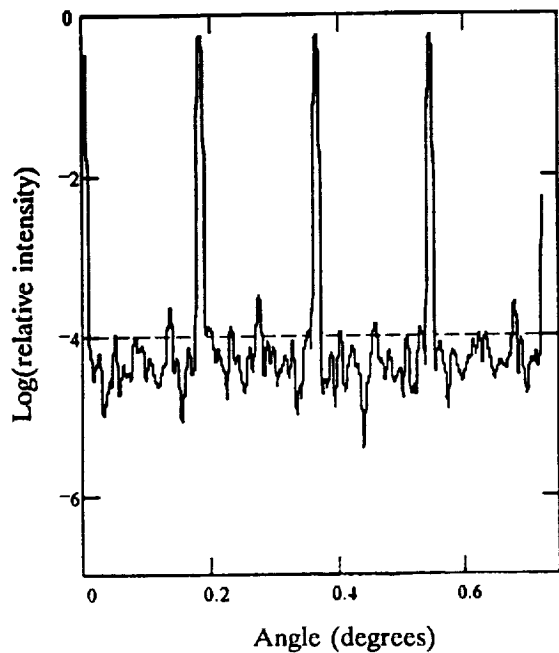


FIGURE 14. Relative intensity, Dammann grating (DG1). Line edge error  $\delta = 1.0 \mu\text{m}$ . Compared to 1-D roughness scattering formula.

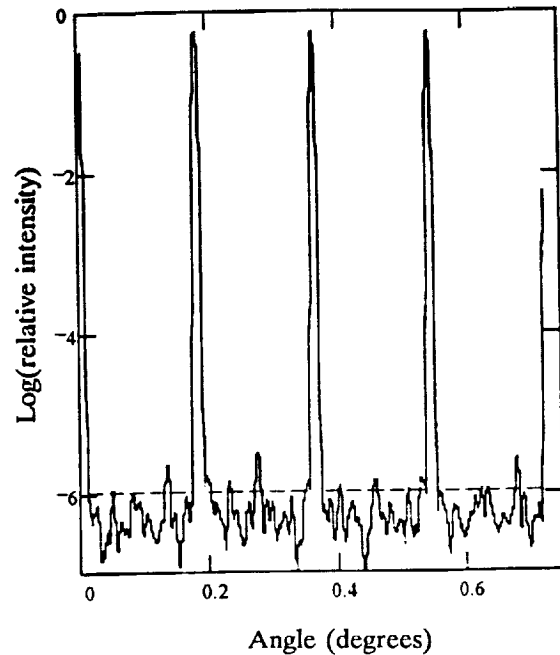


FIGURE 15. Relative intensity, Dammann grating (DG1). Line edge error  $\delta = 0.1 \mu\text{m}$ . Compared to 1-D roughness scattering formula.

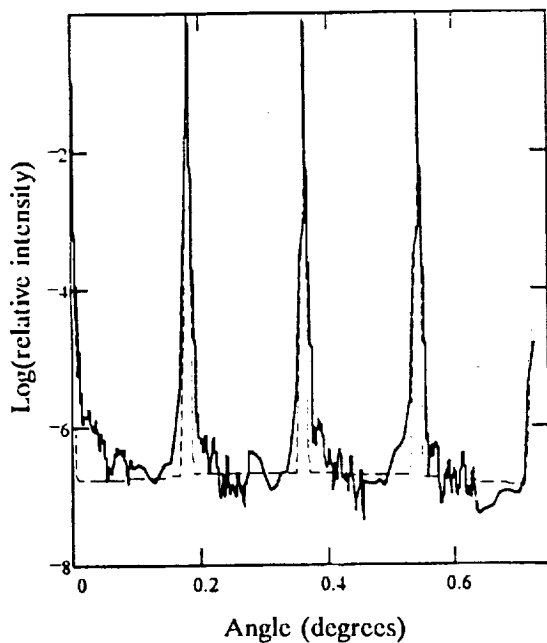


FIGURE 16. Measured relative intensity; compared to 1-D scatter formula with etch depth error  $\delta d = 1 \text{ nm}$ , and line edge error  $\delta x = 25 \text{ nm}$ .

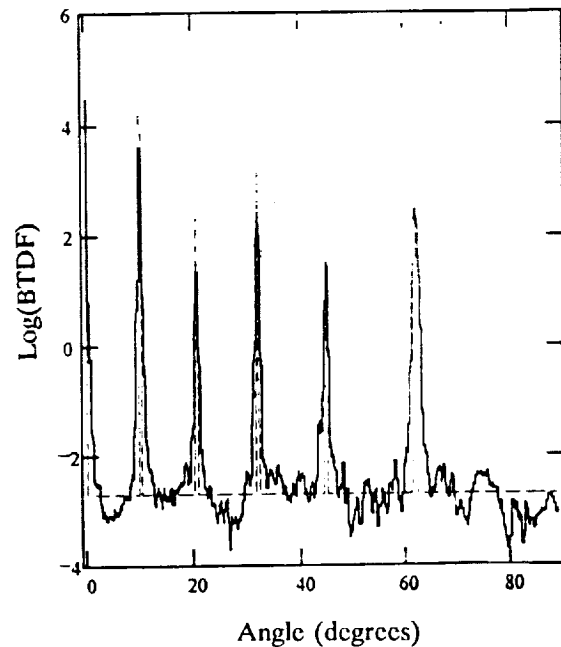


FIGURE 17. Measured BTDF compared to 1-D scatter formula with line edge error  $\delta = 30 \text{ nm}$ .

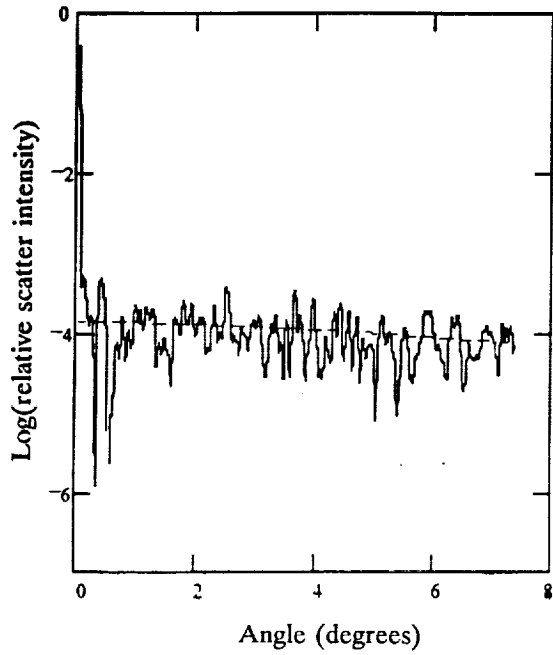


FIGURE 18. Relative scatter intensity, cylindrical Fresnel zone plate (FZP1). Line edge error  $\delta = 1 \mu\text{m}$ . Compared to 1-D roughness scatter formula.

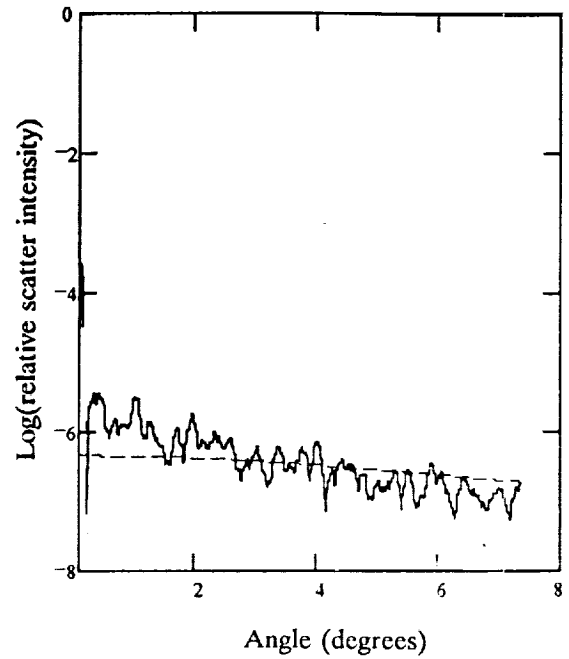


FIGURE 19. Relative scatter intensity, circular Fresnel zone plate (FZP1). Line edge error  $\delta = 1 \mu\text{m}$ . Compared to 2-D scattering formula.